Biophysical *Journal*
Article

Biophysical Society

A Luminal Loop of Wilson Disease Protein Binds Copper and Is Required for Protein Activity

Birgit Köhn,[1,2] Kumaravel Ponnandai Shanmugavel,[3] Min Wu,[3] Michael Kovermann,[1,2,4,*] and Pernilla Wittung-Stafshede[3,*]

[1]Department of Chemistry; [2]Konstanz Research School Chemical Biology, University of Konstanz, Konstanz, Germany; [3]Department of Biology and Biological Engineering, Chalmers University of Technology, Gothenburg, Sweden; and [4]Zukunftskolleg, University of Konstanz, Konstanz, Germany

ABSTRACT The copper-transporting ATPase ATP7B is essential for loading of copper ions to copper-dependent enzymes in the secretory pathway; its inactivation results in Wilson disease. In contrast to copper-ion uptake by the cytoplasmic domains, ATP7B-mediated copper-ion release in the Golgi has not been explored yet. We demonstrate here that a luminal loop in ATP7B, rich in histidine/methionine residues, binds reduced copper (Cu(I)) ions, and identified copper-binding residues play an essential role in ATP7B-mediated metal ion release. NMR experiments on short-peptide models demonstrate that three methionine and two histidine residues are specifically involved in Cu(I) ion binding; with these residues replaced by alanines, no Cu(I) ion interaction is detected. Although more than one Cu(I) ion can interact with the wild-type peptide, removing either all histidine or all methionine residues reduces the stoichiometry to one Cu(I) ion binding per peptide. Using a yeast complementation assay, we show that for efficient copper transport by full-length ATP7B, the complete set of histidine and methionine residues in the lumen loop are required. The replacement of histidine/methionine residues by alanines does not perturb overall ATP7B structure, as the localization of ATP7B variants in yeast cells matches that of the wild-type protein. Thus, in similarity to ATP7A, ATP7B also appears to have a luminal "exit" copper ion site.

INTRODUCTION

Copper (Cu) ions in oxidized (Cu(II)) and reduced (Cu(I)) forms are found in the active sites of many essential proteins that participate in key cellular reactions, often involving electron transfer (1–3). However, because of their redox activity, free Cu ions are potentially toxic for cells because they are capable of producing reactive oxygen species (4). To avoid Cu ion toxicity, the intracellular concentration of Cu ions is regulated via dedicated proteins that facilitate uptake and efflux as well as distribution of Cu ions to Cu-dependent proteins and enzymes (5–7). In the human cytoplasm, after the uptake of Cu(I) ions by the membrane-spanning Ctr1 trimer (8), the small Cu(I) chaperone Atox1 transports the metal to ATP7A and ATP7B (also called Menke's and Wilson disease proteins, respectively), two homologous membrane-bound P_{1B}-type ATPases located in the trans-Golgi network. Once transferred to ATP7A/B, the Cu(I) ion is channeled through the protein into the lumen of the Golgi, where it is loaded onto specific Cu-dependent proteins and enzymes in the secretory pathway.

ATP7A and ATP7B are large (~1400 residues), multidomain proteins with several domains facing the cytoplasm as well as eight membrane-spanning helices that form a channel for Cu(I) (9) (Fig. 1 *A*). Unique to the human homologs, ATP7A and ATP7B have as many as six cytoplasmic metal-binding domains protruding in the cytoplasm. Each metal-binding domain, like Atox1, has a surface-exposed copper-binding motif (10). It is generally assumed that Atox1 delivers Cu(I) to the metal-binding domains of ATP7A and ATP7B that, in turn, transfer the metal to the transmembrane Cu(I) channel in ATP7A/B. With energy from ATP hydrolysis, Cu(I) is thus transferred to the lumen side of the trans-Golgi, where it is loaded onto target proteins coming from the endoplasmic reticulum (ER). Many human copper-dependent enzymes (e.g., blood-clotting factors, tyrosinase, lysyl oxidase, and ceruloplasmin) go via the secretory pathway and depend on either ATP7A or ATP7B for Cu(I) delivery.

In connection to the movement of Cu(I) through the protein, ATP7A/B are likely to undergo significant conformational changes and alterations in domain-domain

Submitted June 27, 2018, and accepted for publication July 30, 2018.

*Correspondence: michael.kovermann@uni-konstanz.de or pernilla-wittung@chalmers.se

Editor: Jill Trewhella.

https://doi.org/10.1016/j.bpj.2018.07.040

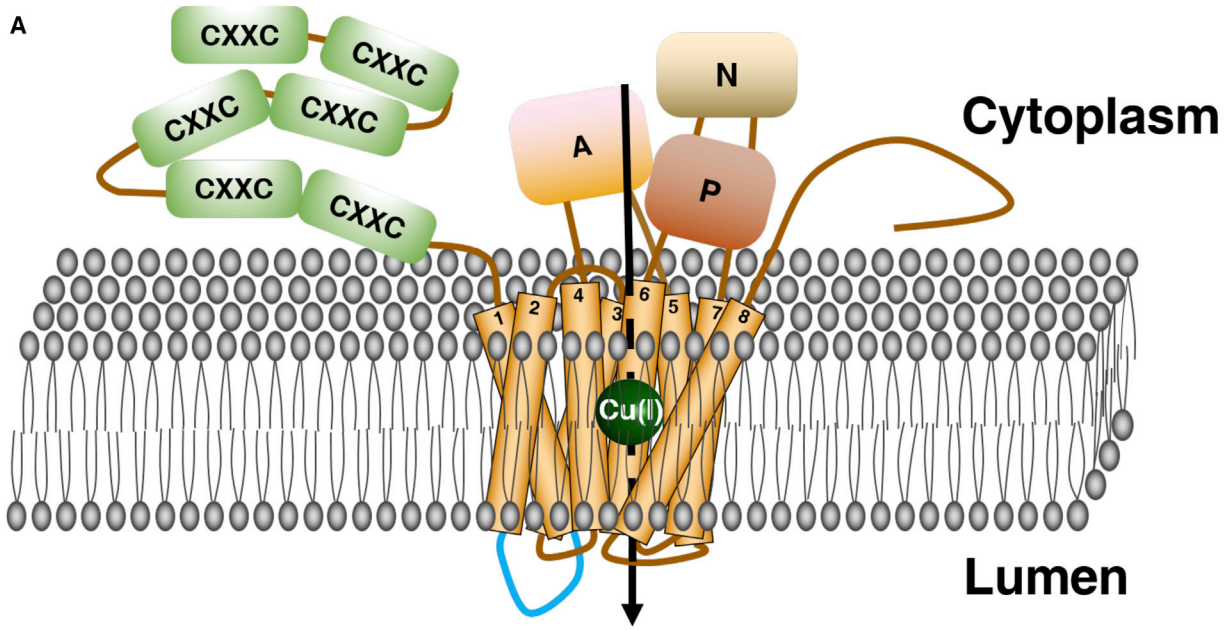

B

		Transmembrane Helix 1 / Lumen loop / Transmembrane Helix 2	
Human ATP7B	654	FLCSLVFGIPVMALMIYMLIPS----------NEPHQSMVLDHNIIPGLSILNLIFFILCTFVQ	707
Human ATP7A	654	FLVSLFFCIPVMGLMIYMMVMDHHFATLHHNQNMSKEEMINLHSSMFLERQILPGLSVMNLLSFLLCVPVQ	724
Legionella pneumophila CopA	85	FWIALMLTIPVVILE--MGG----------HGLKH----FISG-NGSSWIQLLLATPVV	129
Saccharomyces cerevisiae CCC2	262	----TLLAIICMLL--YMIVPMM-WPTIVQ----------DRIFPYKETSFVRGLFYRDILGVILASYIQ	326

C

L-WT	KK-LMIYMLIPSNEPHQSMVLDHNIIP
L-M3A	KK-LAIYALIPSNEPHQSAVLDHNIIP
L-H2A	KK-LMIYMLIPSNEPAQSMVLDANIIP
L-M3H2A	KK-LAIYALIPSNEPAQSAVLDANIIP

FIGURE 1 (*A*) Scheme of domain arrangement in ATP7B. On the cytoplasmic side, there are actuator (A), phosphorylation (P), ATP-binding (N), and six metal-binding (CXXC) domains protruding. On the lumen side, a putative Cu-binding loop (*blue*) is connecting transmembrane helices 1 and 2. (*B*) The alignment of sequences for the lumen segment between helices 1 and 2 in homologs ATP7A, ATP7B, *S. cerevisiae* CCC2, and *L. pneumophila* CopA. Methionine and histidine residues are marked in bold, and the sequence used for NMR experiments is marked in red. (*C*) The primary sequences used in NMR experiments (with KK added to the N-terminus of all to increase solubility, making each peptide 26 residues long). To see this figure in color, go online.

interactions (11). Because there is no high-resolution structural information on the arrangement of the metal-binding domains within full-length ATP7A/B, it is unclear how these domains are arranged relative to each other and to other cytoplasmic domains at different stages of the catalytic cycle. Because Atox1 can deliver Cu(I) to the metal-binding domains through direct protein-protein interactions (12,13), one may speculate that Cu(I)-triggered conformational changes among these domains might initiate the catalytic cycle after Atox1-mediated Cu(I) delivery (14). The metal-binding domains in ATP7B are of high importance for function, as disease-causing point mutations have been found in all six metal-binding domains (15,16), and thus many studies have focused on their roles in the Cu(I) transfer process of ATP7A and ATP7B (17,18).

Less attention has been dedicated to the side of ATP7A/B that faces the lumen and how Cu(I) is delivered to target Cu-dependent proteins in the trans-Golgi network. Because protein synthesis in the secretory path involves several maturation steps in the ER before the protein

reaches the Golgi, most proteins likely have near-native conformations when arriving in the Golgi. ATP7A, but not ATP7B, has a long luminal peptide loop between membrane-spanning helices 1 and 2 that has been reported to contain Cu-binding sites (19) (Fig. 1 *B*). Cu(I) binding to residues in this lumen-protruding segment of ATP7A was proposed to act as an intermediate step before Cu(I) is transferred to a target Cu-dependent protein or released into the vesicular space in the Golgi. Although free Cu ions are toxic in the cytoplasm, in the Golgi vesicles, because of the low pH, both Cu(I) and Cu(II) ions are soluble, and thus the Cu ion uptake mechanism by target proteins may simply be direct binding after release from ATP7A/B. The corresponding segment between helices 1 and 2 in ATP7B is shorter but, upon inspection, also contains putative Cu(I)-binding residues in the form of histidine and methionine residues (20,21). However, there are no studies reported of the role of these residues or this peptide segment in Cu(I) binding and release in ATP7B.

To address this question on a molecular level, we here investigated the Cu(I)-binding capacity of short peptide variants corresponding to the ATP7B luminal segment by in vitro NMR methods. Molecular dynamics simulations were used to assess putative Cu(I)-binding sites populated already in the absence of Cu(I). To place the in vitro findings in a biological context, we used a yeast complementation assay to probe the importance of the identified copper-binding residues in full-length ATP7B Cu transport activity.

MATERIALS AND METHODS

Materials

Peptides were purchased from Innovagen (Lund, Sweden) and contained 26 residues. The wild-type peptide (L-WT; L stands for lumen) holds the primary sequence of KKLMIYMLIPSNEPHQSMVLDHNIIP, whereas the peptide with three Met-to-Ala substitutions (L-M3A) possesses the primary sequence KKLAIYALIPSNEPHQSAVLDHNIIP and the peptide with two His-to-Ala substitutions (L-H2A) has the primary sequence KKLMIYMLIPSNEPAQSMVLDANIIP. The peptide comprising five mutations sites (both three Met and two His residues replaced by Ala, L-M3H2A) exhibits the primary sequence KKLAIYALIPSNEPAQSAVLDANIIP (Fig. 1 *C*). The two N-terminal lysine residues, KK, were added to increase peptide solubility; the following residues in the peptides are labeled as 1 to 24 in the text. Monosodium phosphate (NaH_2PO_4) was purchased from Merck, sodium chloride (NaCl) from VWR, 3-(*N*-morpholino) propanesulfonic acid (MOPS) from Roth, deuterium oxide (D_2O) from eurisotop, hydrochloride acid (HCl, 37% aqueous) from VWR, copper(I) chloride (CuCl) from Sigma-Aldrich (St. Louis, MO), and copper(II) chloride ($CuCl_2$) from Alfa Aesar (Haverhill, MA).

Solution NMR spectroscopy

NMR samples for assignment were prepared in 30 mM NaH_2PO_4, 50 mM NaCl (pH 7.5). NMR samples for the study of Cu(II) interaction contained 53 mM NaCl, 32 mM MOPS, 5% (v/v) D_2O (pH 7.5), and 65 μM of peptide as well as of $CuCl_2$. NMR samples for the study of Cu(I) interaction contained 53 mM NaCl, 32 mM MOPS, 5% (v/v) D_2O (pH 7.5), and either 65 μM or 130 μM of peptide as well as equal or twofold excess of CuCl. To prevent Cu(I) oxidation, CuCl-containing samples as well as stock solutions of CuCl in HCl were prepared under reducing atmosphere (95% N_2, 5% H_2) in airtight NMR tubes. All solutions for anoxic sample preparation were fumigated with N_2 before use. All NMR experiments were recorded on a Bruker 600 MHz spectrometer (Bruker, Billerica, MA) with either a room-temperature probe head or a cryo probe head at $T = 288$ K or $T = 298$ K (diffusion experiment). The assignment of chemical shifts for L-WT was achieved by using two-dimensional homonuclear Overhauser effect spectroscopy (^{1}H-^{1}H NOESY) and total correlation spectroscopy (^{1}H-^{1}H TOCSY) experiments at a concentration of 65 μM peptide. The ^{1}H-^{1}H NOESY spectrum was acquired by using a mixing time of 450 ms and by recording 368 transients, an acquisition time of 131 ms, and a spectral resolution of 2048 data points (spectral width set to 6009 Hz) in the direct and 384 data points (spectral width set to 6009 Hz) in the indirect proton dimension. The ^{1}H-^{1}H TOCSY spectrum was acquired twice by using a mixing time of either 10 or 60 ms and by recording 80 transients, an acquisition time of 341 ms, and a spectral resolution of 4096 data points (spectral width set to 6009 Hz) in the direct and 256 data points (spectral width set to 6009 Hz) in the indirect proton dimension. The assignment of proton resonance signals in L-WT was significantly supported by the acquisition of a two-dimensional heteronuclear ^{1}H-^{13}C HSQC spectrum obtaining ^{13}C chemical shifts increasing the spectral resolution and assisting in identifying the type of amino acid whose chemical shifts have been monitored by the ^{1}H-^{1}H NOESY and ^{1}H-^{1}H TOCSY spectra, respectively. The acquisition of carbon chemical shifts was accomplished by using the natural abundance of the ^{13}C isotope. NMR diffusion experiments were performed using a pulse sequence comprising a stimulated echo assisted by bipolar gradients (22), G, employing a diffusion time, D, of 30 ms and a gradient length, δ, of 6 ms along the z axis. Gradients were calibrated as described in (23). Integrals for proton signals, I, were determined in the spectral range between 0.5 and 2.5 ppm and used for calculation of the diffusion coefficient, D:

$$I(G) = I(0)\exp\left(-G^2\gamma^2\delta^2 D(\Delta - \delta/3)\right),$$

where γ is the gyromagnetic ratio of protons.

Far-ultraviolet CD spectroscopy

All samples for circular dichroism (CD) analysis contained either L-WT or L-M3H2A at a concentration of 30 μM, dissolved in 30 mM NaH_2PO_4 and 50 mM NaCl (pH 7.5), and $T = 288$ K. For analysis, the average of five replicates was used. CD spectra were recorded on a Jasco J-815 CD spectrometer (Jasco, Oklahoma City, OK).

EPR spectroscopy

Three samples were measured using a Bruker EMX Nano X-Band CW spectrometer at room temperature using Quarz tubes (ER221TUB-Q-10). The sample containing buffer only (53 mM NaCl, 32 mM MOPS, 5% (v/v) D_2O at pH 7.5) and the sample containing buffer with 200 μM $CuCl_2$ were prepared under aerobic conditions, whereas the sample containing buffer and 200 μM CuCl was prepared under reducing atmosphere (95% N_2, 5% H_2) in airtight electronic paramagnetic resonance (EPR) tubes. The solution for anoxic sample preparation was fumigated with N_2 before use. The modulation amplitude was set to 8.2 Gauss, and the microwave power was set to 6.31 mW. In total, 50 scans with a measurement time of $\sim$100 s were conducted. A 10-point moving average filter and a third-order polynomial baseline correction were applied. The spectrum representing buffer only was subtracted from the other two spectra containing Cu(I) or Cu(II) ions.

Yeast strains and ATP7B mutant construction

High stress resistance yeast *Saccharomyces cerevisiae* CEN.PK 113-11C (MATa SUC2 MAL2-8 URA3-52 HIS3-Δ1; provided by Dr P. Kötter, Institute of Microbiology, Johann Wolfgang Goethe-University, Frankfurt, Germany) was used as reference strain. Yeast strains were cultivated in liquid yeast extract peptone dextrose media) and grown at 30°C. Yeast strains with CCC2 and ATX1 deletions were used in this study. For the expression of ATP7B and ATOX1 in these yeast strains, plasmids containing human ATP7B (p426GPD) and ATOX1 (p423GPD) were transformed as reported previously (24). The ATP7B luminal loop mutants with all of M668, M671, H679, M682, and H686 mutated to Ala, or only all His mutated to Ala, or only all Met mutated to Ala, or the single mutation M682A, were constructed (Table S1). Mutations were introduced into the full-length ATP7B with a QuikChange site-directed mutagenesis kit using the previously constructed p426GPD-ATP7B plasmid (24) as template. All constructed plasmids were verified by sequencing (Eurofins). DNA primers used for the plasmid construction are listed in Table S2. All plasmids were transformed into yeast cells by the standard lithium acetate method (25).

Yeast growth analysis

ATP7B copper transport activity of the various yeast strains was evaluated using growth curve analysis in iron-limited medium. A single yeast colony from the plates was inoculated in iron-limited medium (SD medium containing 1.7 g/L yeast nitrogen base without Fe and Cu, 50 mM MES buffer (pH 6.1), 20 g/L glucose, 5 g/L ammonium sulfate, complete supplement mixture CSM –Ura –His, 1 mM ferrozine (Fe chelator), 1 μM $CuSO_4$, and 100 μM $FeSO_4$) and incubated over night at 30°C and 200 rotations per minute (18). Yeast cells from this culture were washed with ice-cold deionized water and cultivated in fresh iron-limited medium at an initial optical cell density of $OD_{600} = 0.1$. The growth of the cells was monitored spectroscopically for 30 h. All yeast growth experiments were carried out at identical conditions and in six biological replicates. Growth rates were calculated from the linear exponential growth phase ($\Delta ln(OD_{600})/h$). Mean growth rate was obtained from averaging growth rates of the six replicates, using error propagation to determine the weighted error for each average value.

Western blotting of yeast-expressed ATP7B

Yeast was grown in iron-limited medium for 30 h at 30°C. Cells were spun down by centrifugation at 2000 × *g* at 4°C for 10 min. Cells' pellets were washed twice with ice-cold water and resuspended in lysis buffer (50 mM HEPES (pH 7.5), 150 mM NaCl, 2.5 mM EDTA, 1% v/v Triton X-100, and freshly added protease inhibitor). After disruption with glass beads, membranes were collected by centrifugation at 18,000 × *g* (4°C, 30 min). Samples were resuspended in SDS loading buffer (0.5 M Tris-HCl (pH 6.8), 10% SDS, 0.5% (w/v) bromophenol blue, 87% glycerol, and 100 mM DTT), and 50 mg of membranes were loaded on a 4–12% Bis-Tris gel (Invitrogen, Carlsbad, CA) and blotted onto PVDF membranes. ATP7B variants were detected with monoclonal rabbit ATP7B antibodies (1:1000 dilution; Abcam, Cambridge, UK) upon incubation overnight, followed by incubation with horseradish-peroxidase-conjugated anti-rabbit IgG reagent (Thermo Scientific Pierce, Waltham, MA) for 15 min at 4°C. Bands were visualized by Pierce Fast Western Blot Kits, SuperSignal West Femto, Rabbit (Thermo Scientific Pierce) in a Bio-Rad ChemiDoc analyzer (Bio-Rad, Hercules, CA).

Cell localization of yeast-expressed ATP7B

Yeast cells were cultured to mid-log phase in iron-limited medium. Harvested yeast cells were fixed in 5 mL of 50 mM KPO_4 (pH 6.5), 1 mM $MgCl_2$, and 4% formaldehyde for 2 h. After fixation, the cells were washed two times in 5 mL of PM buffer (100 mM KPO_4 (pH 7.5), 1 mM $MgCl_2$) and followed by resuspension in PMST buffer (100 mM KPO_4 (pH 7.5), 1 mM $MgCl_2$, 1 M sorbitol, 0.1% Triton X-100) to a final OD_{600} of 10. 100 μL yeast cells were incubated for 20 min in 0.6 μL of β-mercaptoethanol and 1 mg/mL zymolyase (Zymo Research, Irvine, CA). The spheroplasted cells were washed with PMST buffer and attached to polylysine-coated coverslips. Adherent cells were blocked in PMST-BSA buffer (0.5% bovine serum albumin (BSA) in PMST buffer) for 30 min. Next, the adherent cells were incubated overnight at 4°C with primary antibody (1:500 rabbit monoclonal ATP7B antibody; Abcam) diluted in PMST-BSA buffer. After incubation, the cells were washed three times with PMST-BSA buffer and incubated with secondary antibody (1:1000 anti-rabbit Alexa 488; Abcam) for 3 h at room temperature and with 0.4 mg/mL DAPI (staining nuclei) for 5 min. Cells were mounted in Vectashield mounting medium (Vector Laboratories, Burlingame, CA). Images were acquired using a Leica DM 2000 inverted microscope (Leica, Wetzlar, Germany) and processed with the Leica application suite (LAS-AF lite) software.

Homology ATP7B model and molecular dynamics simulation

The sequences of human ATP7B (isoform 1, P3567041, 1465 residues) were retrieved from the UniProt database (26). The transmembrane segments of human ATP7B were predicted using the TMHMM server (27). Homology models of $ATP7B^{654–707}$ and $ATP7B^{654–1378}$ were built with the x-ray structure of *Legionella pneumophila* CopA as the template (3RFU (28)) through the Phyre^2 server (29). The $ATP7B^{654–707}$ construct contains transmembrane helices 1 and 2 and the connecting lumen-protruding loop. The $ATP7B^{654–1378}$ construct contains eight transmembrane segments, the lumen side loops, and the cytoplasmic A, P, and N domains. Molecular dynamics (MD) simulations were performed for the $ATP7B^{654–707}$ construct with protonation states of charged side chains predicted by PDB2PQR server (30). The protein segment was inserted in a lipid membrane comprising dipalmitoylphosphatidylcholines (DPPC) (obtained from the Biocomputing Group at University of Calgary (31)) by InflateGRO methodology (32). The final system contained 125 DPPC lipids solvated by 4062 water molecules and was neutralized with Na^+ and Cl^- ions (Fig. 2). The GROMACS simulation package 5.0.4 (33) was employed for the MD simulation. The system was energy minimized, followed by a 0.1 ns NVT run at $T = 323$ K—which is above the DPPC gel-fluid phase transition (34)—and then the DPPC membrane was allowed to adjust to the protein through 30 ns NPT runs in which protein heavy atoms were restrained. The resulting system acted as a starting point for a 150 ns NPT run in which the heavy atoms' spatial restrictions on the lumen-side loop (residues 667–690) were removed. The simulation was performed using the OPLS-AA force field (35) for protein and Berger lipid parameters (36) modified to be consistent with OPLS conventions (37). The SPC water model (38) was employed. The steepest-descent method was used for simple energy minimization. The NVT run was performed at $T = 323$ K through a Velocity-rescale thermostat (39) using the Nosé-Hoover thermostat (40,41) and the Parrinello-Rahman barostat (42,43) for temperature (323 K) and pressure ($p = 1$ bar) couplings. A semi-isotropic pressure coupling was used to achieve pressure equilibration because of the presence of the membrane. A time step of 2 fs was used together with LINCS constraints (44). Van der Waals and electrostatic interactions were implemented with a cutoff at 1.2 nm, and long-range electrostatic effects were treated by particle mesh Ewald (45) using a fast Fourier transform grid spacing of 0.16 nm. Atomic coordinates and the energy values were saved every 10 ps.

RESULTS

Peptide model of lumen segment is monomeric and unstructured in solution

To obtain residue-specific insights into putative Cu(I) ion interactions with the lumen peptide segment of ATP7B,

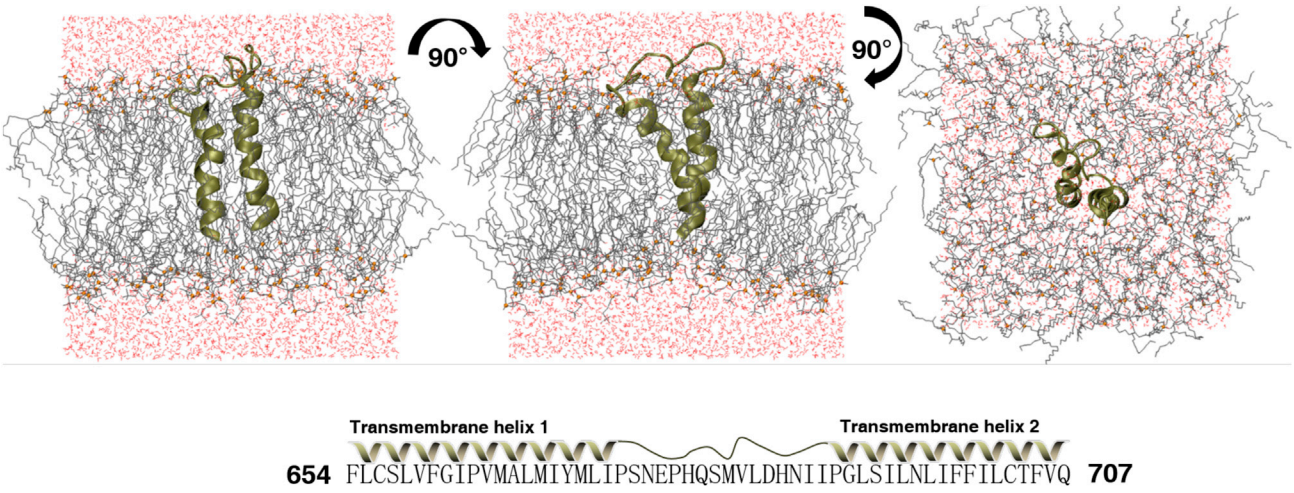

FIGURE 2 The initial system for MD simulations. The protein segment included is shown in cartoon, with lipids and water molecules displayed in line as well as the lipids' phosphorus atoms in beads. The bottom shows the amino acid sequence of the used ATP7B$^{654–707}$ segment illustrated with secondary structure motifs. To see this figure in color, go online.

high-resolution NMR spectroscopy was employed with a 26-residue peptide model (sequence in Fig. 1 *C*). The ATP7B lumen peptide segment inherently contains three methionine (M2, M5, and M16) and two histidine (H13 and H20) residues that all are putative Cu(I)-binding residues (the first two N-terminal lysine residues, KK, in the peptides are not numbered, so the following residues are labeled 1–24). The one-dimensional proton NMR spectrum of the ATP7B luminal peptide model (L-WT) shows a distribution of chemical shifts as expected for an unstructured peptide of this size (Fig. 3 *A*). In Fig. 3 *B*, only the chemical shifts for aromatic and side-chain peptide resonances are shown along with the identifications of the signals from residues Y4, H13, and H20. Importantly, this particular spectral range enables us to specifically monitor the resonances from the two histidine and single tyrosine residues in the peptide in the subsequent copper interaction studies (see below). By focusing on a prominent part of the one-dimensional NMR spectrum, the analysis of the interaction between Cu(I) and the luminal ATP7B segment is made clearer.

The partial assignment of proton chemical shifts of the L-WT peptide has been accomplished by classical two-dimensional homonuclear ^{1}H-^{1}H NOESY and ^{1}H-^{1}H TOCSY (Fig. S1 *A*) experiments (Table S3). The acquisition of a two-dimensional ^{1}H-^{13}C HSQC spectrum increased the spectral resolution and provided significant support to the assignment of proton resonance signals (Fig. S1 *B*). The far-ultraviolet CD spectrum of L-WT peptide (Fig. S2) supports the conclusion of a random-coil-like structure, as indicated by the one-dimensional proton NMR spectrum. Moreover, using NMR diffusion experiments, a diffusion coefficient of $D = (1.45 \pm 0.01) \times 10^{-10}$ m^2 s^{-1} was determined for L-WT (Fig. S3 *A*). This value corresponds to a hydrodynamic radius of about $r_H = 16.7$ Å and is in good accordance with a value of $r_H = 14$ Å that can be calculated for an unstructured monomeric peptide comprising 26 residues (46). We note that an unstructured trimeric 26-residue peptide (total of 78 residues) would correspond to an estimated hydrodynamic radius of $r_H = 26$ Å (46). Thus, the L-WT peptide appears to be monomeric and unstructured in solution.

Peptide model of lumen segment displays specific Cu(I) binding

Next, one-dimensional proton as well as two-dimensional heteronuclear ^{1}H-^{13}C HSQC NMR spectroscopy was applied to probe potential copper interaction with the L-WT peptide.

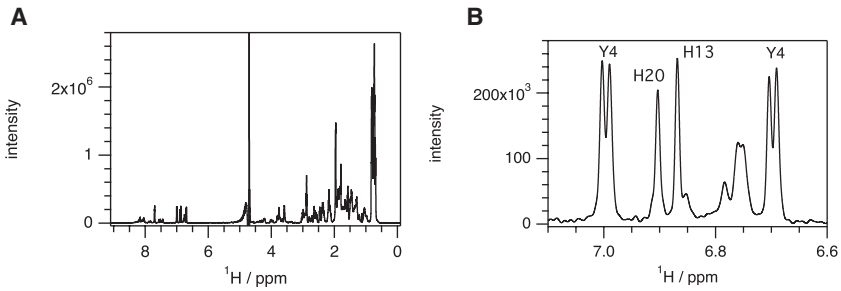

FIGURE 3 One-dimensional proton NMR spectra for L-WT peptide. (*A*) Chemical shifts for all protons comprising the wild-type peptide are shown. (*B*) Chemical shifts comprising selected aromatic and side-chain resonances only are shown. The associated assignment is shown by using the one-letter code for amino acids following position in primary sequence. All chemical shifts that have been assigned are listed in Table S3.

Upon addition of Cu(II), i.e., the oxidized and not biologically relevant oxidation state, we found significant changes in the chemical shift pattern dominated by a significant increase in linewidth of the L-WT peptide resonances (Fig. S4 *A*), followed by a pronounced peptide precipitation. Because the biological relevant form of copper when traveling through ATP7B is Cu(I) (19), i.e., the reduced state of copper, we focused on this redox state (using strict anaerobic conditions to keep the Cu ion reduced at all times) in subsequent experiments. Notably, control experiments using EPR spectroscopy assured that the conditions used in NMR experiments kept the Cu(I) ions in the reduced state (Fig. S5).

The presence of Cu(I) ions induces several changes in the proton one-dimensional NMR spectrum of the L-WT peptide (Fig. 4). Specifically, the H20 aromatic signal disappears and the H13 aromatic signal is decreased upon Cu(I) addition, but there is no effect on the Y4 (next to putative Cu ligand M5) resonances, neither in the chemical shift nor in the linewidth data. Increasing amounts of Cu(I) (from 1:1 to 2:1 Cu(I)/peptide stoichiometry) amplify the changes in NMR chemical shifts (Fig. 4) such that the histidine resonances are altered further and residue Y4 also becomes slightly affected. Two-dimensional heteronuclear ^{1}H-^{13}C NMR spectroscopy corroborates the proposed interaction between Cu(I) and the methionines in L-WT as the methionine methyl group signals disappear upon Cu(I) addition (Fig. S4 *B*). Hence, the NMR data imply the presence of more than a single Cu(I) binding site in the L-WT peptide. We did not determine the affinity value of the interaction of Cu(I) to the peptide, as such experiments are nontrivial (47), and regardless, such a value would not provide much biological relevance, as the system under study is a peptide model. Nevertheless, our result of stoichiometric binding at the concentrations used implies that the dissociation constant for Cu(I) to L-WT peptide binding has to be in the low micromolar range or below.

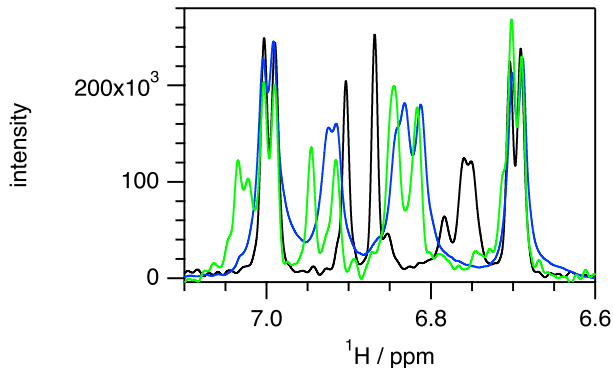

FIGURE 4 One-dimensional proton NMR spectra for L-WT in absence (colored in *black*) and in presence of one Cu(I) ion (colored in *blue*) or two Cu(I) ions per peptide (colored in *green*), respectively. The assignment of the chemical shifts for the wild-type peptide is shown in Fig. 3 *B*. To see this figure in color, go online.

The determination of the diffusion property of the L-WT peptide in the presence of 1:1 and 2:1 Cu/peptide stoichiometry illuminates that the monomeric state of the peptide remains with Cu(I) (Fig. S3, *B* and *C*). The diffusion coefficient for a stoichiometry of one Cu(I) ($D = (1.45 \pm 0.01) \times 10^{-10}$ m^2 s^{-1}, Fig. S3 *B*) or two Cu(I) per peptide ($D = (1.55 \pm 0.02) \times 10^{-10}$ m^2 s^{-1}, Fig. S3 *C*) is similar to the value determined in absence of Cu(I). Thus, the wild-type peptide can bind at least two Cu(I) ions while remaining in a monomeric state in solution.

Tentative Cu(I) binding sites in lumen peptide predicted in silico

To probe the conformational landscape of the lumen peptide in silico, we built a model that included the connecting transmembrane helices (in total, containing residues 654–707) and a piece of a membrane, as described in Materials and Methods. In this model, the loop segment was predicted to have a disordered structure and was positioned protruding from the membrane. H679 and H686 and M668, M671, and M682 are residue numberings that refer to the full-length ATP7B sequence, and these correspond to H13 and H20 and M2, M5, and M16 in the model peptide investigated by NMR spectroscopy.

During the 150 ns simulation, the disordered structure of the protruding peptide segment was retained. The covariance matrix together with principal component analysis (PCA) was used to pinpoint dominating conformational ensembles populated during the simulation. When the simulation data were projected along the largest eigenvector-eigenvalue pairs (Fig. 5 *A*), three major conformational states, termed clusters I (first 18 ns), II (next 10 ns), and III (last 122 ns), are revealed (Fig. 5 *B*). The cluster I ensemble has M668, M671, and H679 close to each other. In cluster II, M671, H679, and M682 are close together, and in the most long-lived structural ensemble, cluster III, M668, M671, and M682 are close to each other. These computational results demonstrate that putative Cu(I)-binding sites in the luminal peptide involving His and Met residues are partially populated already in the absence of metal. Although Cu(I) binding would stabilize the putative metal sites dramatically, it is not uncommon that ligand-binding sites and ligand-bound protein structures are partially populated at equilibrium also in the absence of ligand. This "conformational selection" mechanism is found to be compatible with many enzymes (48,49).

Key roles of histidines and methionines for Cu(I)-peptide interaction in vitro

To address the particular role of the two histidine (H13 and H20) and three methionine (M2, M5, and M16) residues in the lumen peptide segment, we additionally investigated

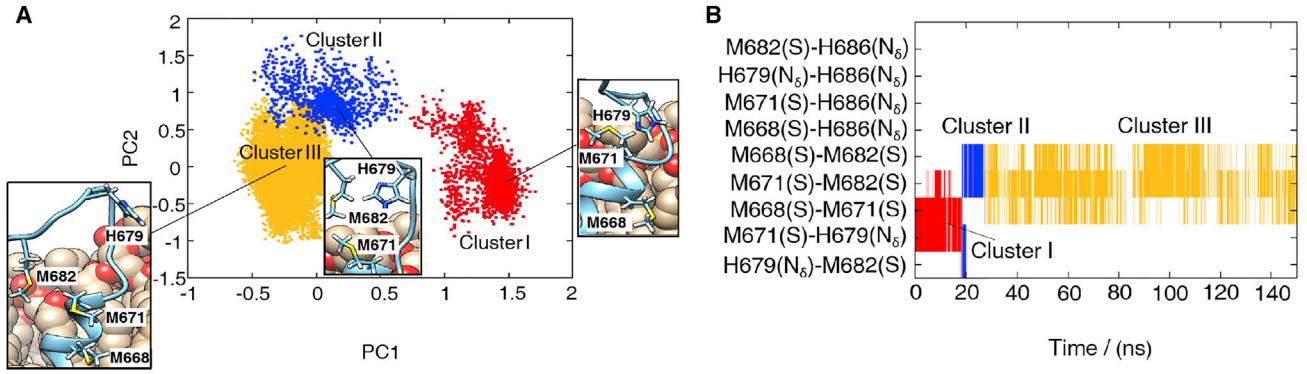

FIGURE 5 (*A*) The principal component analysis on the WT ATP7B$^{654–710}$ domain. The 150 ns MD trajectories are projected on the two most significant principal components of the first lumen-protruding loop Cα atoms' covariance matrix. The first component corresponds to the *x* axis, and the second corresponds to the *y* axis. All the snapshots are grouped into three clusters: cluster I (*red*), cluster II (*blue*), and cluster III (*yellow*). A relevant structure from each cluster is shown in cartoon with residues Met/His in stick and DPPC molecules in sphere. (*B*) The distances among two His (H679 and H686) residues' N$_\delta$ atoms and three Met (M668, M671, and M682) residues' S atoms along the simulation time. All distance values are larger than 0.3 nm. The distance values <0.6 nm are displayed as lines colored according to the clusters: cluster I in red, cluster II in blue, and cluster III in yellow. To see this figure in color, go online.

three mutated peptide variants (Fig. 1 *C*) by NMR spectroscopy.

First, replacement of the two histidine residues with alanine residues (L-H2A peptide) induces only slight changes in the chemical shift pattern of the peptide in its apo form (Fig. S6, *A* and *B*), but the ability to interact with stoichiometric amounts of Cu(I) is retained (Fig. S6 *C*). For this variant, Cu(I) addition shifts the aromatic resonances of Y4 somewhat, which implies that M5 is affected. However, increasing the amount of Cu(I) ions to two Cu(I) per peptide does not induce further changes in the chemical shift pattern of the L-H2A variant (Fig. S6 *C*), indicating the presence of a single binding site that is already saturated by the first equivalent of Cu(I) added. This result is in clear contrast to the finding that the addition of two Cu(I) ions to the WT-L peptide induces additional changes in the chemical shifts as compared to addition of one Cu(I) equivalent.

Moreover, the replacement of the three methionine residues with alanine residues (L-M3A peptide) induces again only slight changes in the chemical shift pattern of the peptide itself (Fig. S7, *A* and *B*) but preserves the ability to interact with one equivalent of Cu(I) (Fig. S7 *C*). When a Cu(I) ion is added to this peptide variant, there is no effect on the aromatic resonances of Y4 (which is reasonable, as the putative copper-binding site M5 has been replaced with an alanine), but the aromatic signals representing H20 and H13 in essence disappear completely. Again, an increasing amount of Cu(I) ions (to two Cu(I) per peptide variant) does not induce further changes in the chemical shift pattern of the L-M3A variant (Fig. S7 *C*), indicating the presence of a single binding site, as observed for the L-H2A variant. Moreover, this binding site is saturated by the first Cu(I) equivalent added, suggesting a dissociation constant below the low micromolar range. The determination of the diffusion coefficient $D = (1.43 \pm 0.01) \times 10^{-10}$ m^2 s^{-1} for the L-M3A peptide variant in the presence of Cu(I) (Fig. S3 *D*) confirms again the monomeric character of the peptide even when it is bound to the metal ion.

Using a third peptide variant, L-M3H2A, both the two histidine and three methionine residues have been replaced by alanine residues, providing a peptide with five substituted amino acids in total lacking the putative intrinsic binding sites for Cu(I). NMR spectroscopy illuminates that L-M3H2A retains the structural characteristics of L-WT peptide, as exemplarily seen for aromatic protons belonging to Y4 (Fig. S8). Impressively, addition of a stoichiometric amount of Cu(I) ions per L-M3H2A peptide variant does not result in any changes in the chemical shift pattern (Fig. 6), indicating that the removed five side chains (or a subset thereof) are essential for the L-WT peptide interactions with Cu(I) when the concentrations are in the low micromolar range.

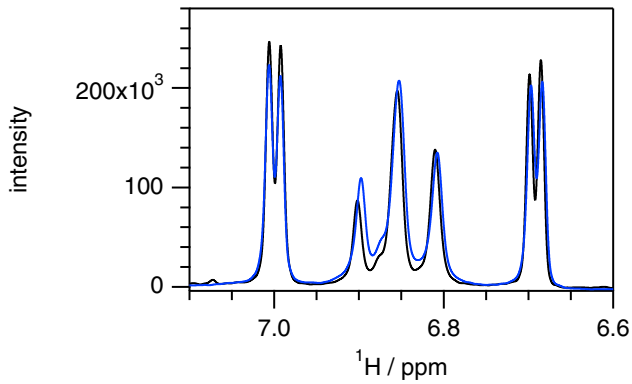

FIGURE 6 One-dimensional proton NMR spectra for the five-residue variant L-M3H2A in absence (colored in *black*) and in presence of a one Cu(I) ion per peptide (colored in *blue*). The assignment of the chemical shifts for the wild-type peptide is shown in Fig. 3 *B*. To see this figure in color, go online.

Combining the results, Cu(I) appears capable of interacting with both histidine and methionine residues in the L-WT peptide, and more than one Cu(I) ion can bind to one L-WT peptide. In contrast, when the Cu(I) interaction site is limited to only methionine (L-H2A variant) or only histidine residues (L-M3A variant), only one Cu(I) ion per peptide binds. Consequently, the interaction of Cu(I) with the peptide is totally abolished upon replacing both the methionine and histidine residues with alanine residues (L-M3AH2A variant). Notably, because the chemical shift pattern changes observed when Cu(I) was added to L-WT peptide do not match the changes found when Cu(I) was added to either one of the two peptide variants, the Cu(I) interaction sites in the L-WT peptide likely comprise a combination of histidine and methionine residues. Accordingly, the MD simulation suggested two putative metal-binding sites, clusters I and II, that contain both His and Met residues.

Role of lumen segment residues for in vivo Cu transport activity

To test the role of the putative Cu-binding residues in full-length ATP7B, we turned to a yeast complementation assay (50). The concept builds on the fact that yeast requires Cu ions as cofactors in Fet3p (the yeast homolog of human ceruloplasmin) to survive in iron-limiting conditions. Fet3p obtains its Cu ions from the pathway involving the yeast Atox1 homolog, Atx1p, and the yeast ATP7A/B homolog, CCC2p. We recently set up a system involving the deletion of yeast genes for CCC2p and Atx1p and supplementation with the human genes for Atox1 and ATP7B on high-copy plasmids that allowed for testing variants of ATP7B (24). Here, we took advantage of this established system and, in similarity to the NMR experiments, introduced mutations of the putative Cu(I)-binding residues in the luminal segment in the full-length protein.

The growth rates (in exponential phase) for ΔCCC2ΔAtx1 yeast strains with different ATP7B variants added on plasmids (Table S1) were probed in combination with the wild-type Atox1 gene in iron-limited conditions (Figs. 7 *A* and S9 *A*). First, as expected, without Atx1p and CCC2p genes and no added human genes, the resulting yeast grow poorly, whereas when the wild-type proteins ATP7B and Atox1 genes are supplied on plasmids to the ΔCCC2ΔAtx1 yeast strain, the growth rate matched that of yeast with the normal yeast genes present. Importantly, when ATP7B plasmids with mutations were introduced to the ΔCCC2ΔAtx1 yeast strain (with wild-type Atox1 in all cases), the resulting growth rates depended on the specific mutations introduced but were all found between the lowest (no ATP7B plasmid added to the ΔCCC2ΔAtx1 yeast) and the highest value (plasmid with wild-type ATP7B added).

When the three methionine and two histidine residues in the lumen loop were exchanged for alanine in the ATP7B construct, the yeast growth roughly matched that found for yeast without copper-transport genes, i.e., the ΔCCC2ΔAtx1 yeast strain without added plasmids (Fig. 7 *A*). Thus, because yeast growth (in the exponential phase) correlates with copper-transport efficiency, there appears to be no copper transport for this ATP7B variant. When only histidine (H2A) or only methionine (M3A) were exchanged for alanine in ATP7B, yeast growth was reduced but not fully abolished. Notably, the effect on yeast growth (i.e., copper transport) was larger for M3A than for H2A ATP7B (Fig. 7 *A*), implying a more prominent role of the methionine residues in mediating luminal copper exit. When only one methionine was replaced with alanine (M682A) in ATP7B, almost no effect on growth was observed. Thus, removing only one methionine residue did not perturb ATP7B's ability to transport copper to Fet3p much.

Western blot analysis confirmed that all ATP7B variant proteins are expressed in similar amounts as wild-type ATP7B in the yeast cells when grown in iron-limited medium (Fig. S9 *B*). Moreover, analysis of the localization of the ATP7B variants in the yeast cells by immunostaining demonstrates that the mutants, like wild-type ATP7B, clearly leave the ER and are found throughout the cells (Fig. 7 *B*). The expressed ATP7B proteins are all distributed throughout the yeast cells in a dispersed pattern. If ATP7B mutants had been trapped in the ER because of improper folding, this would show as distinct immunostaining surrounding the nucleus (nuclei stained with DAPI in Fig. 7 *B*). Thus, the introduced mutations in the luminal loop do not affect the biosynthesis (expression, folding, and distribution) of full-length ATP7B. Accordingly, on a local scale, the NMR data demonstrate that the introduced mutations do not significantly affect the structure of the luminal peptide model. Thus, it is reasonable to conclude that the observed differences in yeast growth for the variants is due to defects in ATP7B-mediated copper transport and not to less expressed protein or the protein being trapped in the ER. Therefore, the mutated residues in the lumen loop are required for efficient ATP7B-mediated copper transport.

DISCUSSION

To begin to investigate Cu release by ATP7B, we here assessed the presence of Cu(I) binding sites in a luminal segment of ATP7B between transmembrane helices 1 and 2 (Fig. 1). We used four 26-mer peptides for NMR spectroscopic experiments differing in the number of potential copper-interacting side chains. We are aware that, in the full-length protein, the ends of this peptide stretch are confined in helices 1 and 2, thereby forming a protruding loop into the lumen (and mimicked in the computations; Fig. 2). Thus, it must be acknowledged that in-vitro-detected Cu-binding sites and Cu affinities (which we therefore did not determine) may not be identical in the free-peptide

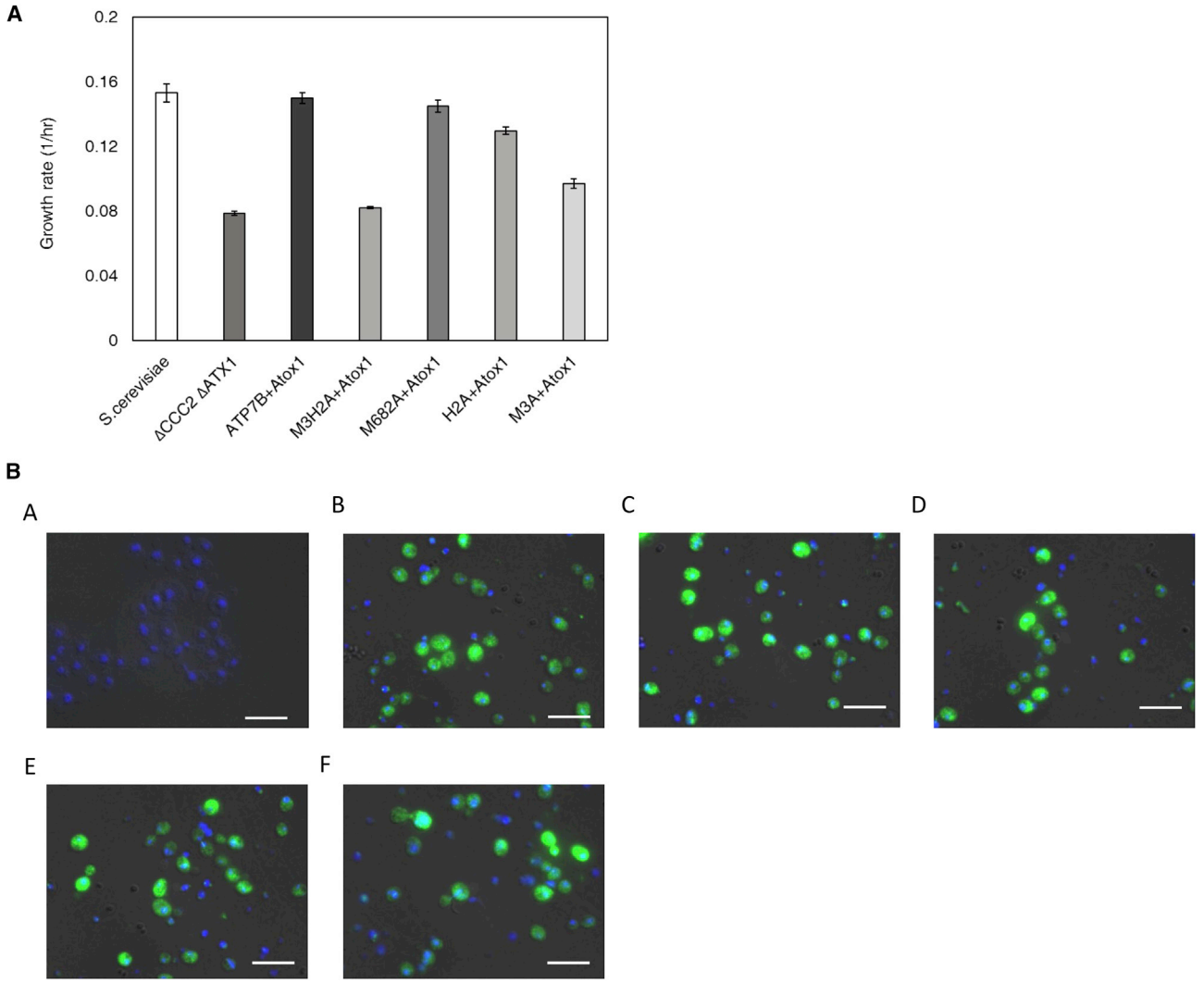

FIGURE 7 (*A*) Growth rates (shown as *bars*, *y* axis) of the ΔCCC2ΔAtx1 yeast strain complemented with high-copy plasmids with wild-type Atox1 and ATP7B variants, as indicated on *x* axis, in iron-limited conditions (*bars* show weighted average ± error). Error bars are based on weighted error from six biological replicates. (*B*) The immunostaining of ATP7B variants in yeast cells using ATP7B-specific antibodies. Nuclei were visualized by DAPI staining. Scale bars, 10 μm. Each image shows: (*a*) ΔCCC2ΔAtx1 yeast without ATP7B plasmid as control; (*b*) with wild-type ATP7B high-copy plasmid; (*c*) the H2A ATP7B variant; (*d*) the M3A ATP7B variant; (*e*) the M682A variant, and (*f*) the M3H2A ATP7B variant. To see this figure in color, go online.

system as in the full-length protein in vivo. Nonetheless, we detect stoichiometric binding of one and two Cu ions per L-WT peptide in solution showing an affinity for Cu(I) ions in the micromolar concentration range (or below), and the L-WT peptide remains monomeric, as quantitatively determined by diffusion NMR methodology.

For the two peptide variants used, lacking either two histidine or three methionine residues, only one Cu(I) ion per peptide is able to bind, but the interaction remains stoichiometric, and thus affinity is still in the low micromolar (or even below) concentration range and the peptide-Cu(I) complexes stay monomeric. Even if the peptide system studied here differs from the scenario in vivo, several implications can be made from the results as obtained by the application of high-resolution NMR spectroscopy when combined with the in vivo analysis of full-length ATP7B variants.

Most dramatic is the conclusion that the variant with five replacements with alanine residues (i.e., no methionine and no histidine residues present) cannot bind Cu(I) (Fig. 6), and these mutations introduced in full-length ATP7B abolish copper transport in yeast (Fig. 7). Because the mutated H2A and M3A ATP7B variants are less efficient than wild-type ATP7B in copper transport in yeast but the NMR spectroscopic data show that L-H2A and L-M3A still interact with one Cu(I), the specific Cu(I)-binding site (i.e., identity and position of coordinating residues) or the actual number of Cu(I) ions bound (one or more ions) are of crucial importance for proper ATP7B function. In the wild-type peptide, L-WT, it appears that Cu(I) interacts with a combination of histidine and methionine residues presenting more than a single Cu(I)-binding site. The latter is also supported by the MD simulations (in the absence of copper) that revealed partially populated

metal-binding sites in the lumen segment that involved both methionine and histidine residues (clusters I and II; Fig. 5).

Putative interactions between the lumen side of ATP7B and the target protein ceruloplasmin have been proposed (51). Ceruloplasmin variants with point mutations in loop regions were found to not be copper loaded by ATP7B, but CCC2p could load Cu ions to these variants without problems. This result indicated that ceruloplasmin loops play critical roles in Cu ion incorporation in the lumen. In addition, the authors proposed that the process of Cu ion loading in yeast versus mammalian cells is less structurally demanding or the two Cu(I)-transporting ATPases differ in their structures on the luminal side (51).

In contrast to the lack of homology between the lumen segments of ATP7B and CCC2p (Fig. 1 *B*), this segment shows some homology when comparing ATP7B with ATP7A. A Met/His-enriched lumen loop between helices 1 and 2, as found in ATP7B, is also present in ATP7A. This lumen peptide in ATP7A also has a Met/His stoichiometry of roughly two, but the ATP7A loop is ~18 amino acids longer than in ATP7B and has in total more Met/His residues (19) (Fig. 1 *B*). For ATP7A, it was shown that mutations of histidine and methionine residues in the lumen loop did not prevent ATP7A phosphorylation, but such mutations inhibited dephosphorylation and copper ion release (19). In addition, upon inserting the loop peptide into a scaffold protein, two distinct Cu(I)-binding sites were suggested (19), which both involved mixed histidine and methionine residue coordination in similarity to what we discovered here for ATP7B. We note, however, that in the ATP7A study (19), the lumen loop was modeled to have a helical structure (the authors did not perform MD simulations), whereas we made the protruding loop start with an unstructured conformation in the MD simulations of the loop connected to helices 1 and 2. Recently, a cryo-EM structure of ATP7B was reported, and it was found that ATP7B formed stable dimers (52). Analysis of the reported dimer structure reveal that the luminal loops do not form contacts and this, together with our NMR spectroscopic data demonstrating that the peptides remain monomeric with Cu(I), implies that Cu binding to the luminal part of ATP7B likely takes place intramolecularly.

To speculate how the transfer pathway of Cu(I) through ATP7B may be linked to the discovered Cu(I)-binding sites in the lumen peptide, we created a homology model of human ATP7B$^{654–1378}$ that consisted of the eight helical transmembrane domains and the cytoplasmic A, P, and N domains. Our model was made in the same way as reported and is in essence identical to the previously published ATP7B model (53,54). In the previous analysis, the copper release pathway was suggested to include three sequential copper-binding sites: an entry copper site, a central copper-binding site, and a copper exit site (53). The entry copper site includes residue M729 and several charged residues (D730, R778, E781, and D918), cf. Fig. S10 *A*; the central copper-ion-binding site includes the conserved CPC-motif, cf. Fig. S10 *B*; and the proposed copper ion exit site is centered on residue D765 plus four nearby methionine residues (Fig. S10 *C*). In addition to these sites, which are also obvious in our model, we propose a final exit copper ion site in ATP7B that involves residues in the lumen peptide (Fig. S10 *D*). This copper-ion-binding site or set of sites likely involves a subset of the five identified copper-coordinating residues M668, M671, H679, M682, and H686, as jointly supported by our in vitro NMR, in vivo yeast, and in silico computational results.

To conclude, by using various biophysical methods, we have shown that the lumen peptide of ATP7B can specifically bind Cu(I) ions using histidine and methionine residues in similarity to the corresponding but longer segment in ATP7A. Thus, like ATP7A, ATP7B appears to have a luminal "exit" copper ion site that helps transfer the Cu(I) ions from binding sites within the membrane-spanning channel to the lumen side of the Golgi. One may speculate that target proteins to be loaded with copper ions in the Golgi obtain Cu(I) ions from these exit sites via direct protein-protein interactions, although no such studies have yet been performed. Notably, in corresponding chloroplast P_{1B-1}-type ATPases HMA6 and HMA8, conserved Cu(I)-interacting (here, His and Cys residues) positions have also been described in transmembrane helix 1 and the following lumen-protruding peptide segment that appear important for Cu(I) release in the chloroplasts (55).

SUPPORTING MATERIAL

Ten figures and three tables are available at http://www.biophysj.org/biophysj/supplemental/S0006-3495(18)30935-4.

AUTHOR CONTRIBUTIONS

P.W.-S. and M.K. designed the study. B.K., K.P.S., M.W., and M.K. performed experiments and analyzed data. P.W.-S and M.K. wrote the manuscript. All authors edited the text.

ACKNOWLEDGMENTS

We thank Istvan Horvath for technical aid, Patrick Roser for support with EPR, and Stefan Kreft for fruitful discussion.

This work is supported by the Swedish Research Council (P.W.-S), the Knut and Alice Wallenberg Foundation (P.W.-S), the Young Scholar Fund (M.K.), and the Zukunftskolleg hosted in Konstanz (M.K.). Computing time at the C3SE Supercomputing Center (Chalmers) through the Swedish National Infrastructure is acknowledged.

REFERENCES

1. Huffman, D. L., and T. V. O'Halloran. 2001. Function, structure, and mechanism of intracellular copper trafficking proteins. *Annu. Rev. Biochem.* 70:677–701.

2. Puig, S., and D. J. Thiele. 2002. Molecular mechanisms of copper uptake and distribution. *Curr. Opin. Chem. Biol.* 6:171–180.
3. Harris, E. D. 2003. Basic and clinical aspects of copper. *Crit. Rev. Clin. Lab. Sci.* 40:547–586.
4. Valko, M., H. Morris, and M. T. Cronin. 2005. Metals, toxicity and oxidative stress. *Curr. Med. Chem.* 12:1161–1208.
5. O'Halloran, T. V., and V. C. Culotta. 2000. Metallochaperones, an intracellular shuttle service for metal ions. *J. Biol. Chem.* 275:25057–25060.
6. Festa, R. A., and D. J. Thiele. 2011. Copper: an essential metal in biology. *Curr. Biol.* 21:R877–R883.
7. Robinson, N. J., and D. R. Winge. 2010. Copper metallochaperones. *Annu. Rev. Biochem.* 79:537–562.
8. Ohrvik, H., and D. J. Thiele. 2014. How copper traverses cellular membranes through the mammalian copper transporter 1, Ctr1. *Ann. N. Y. Acad. Sci.* 1314:32–41.
9. Lutsenko, S., E. S. LeShane, and U. Shinde. 2007. Biochemical basis of regulation of human copper-transporting ATPases. *Arch. Biochem. Biophys.* 463:134–148.
10. Boal, A. K., and A. C. Rosenzweig. 2009. Structural biology of copper trafficking. *Chem. Rev.* 109:4760–4779.
11. Lutsenko, S., N. L. Barnes, …, O. Y. Dmitriev. 2007. Function and regulation of human copper-transporting ATPases. *Physiol. Rev.* 87:1011–1046.
12. Niemiec, M. S., A. P. Dingeldein, and P. Wittung-Stafshede. 2015. Enthalpy-entropy compensation at play in human copper ion transfer. *Sci. Rep.* 5:10518.
13. Niemiec, M. S., C. F. Weise, and P. Wittung-Stafshede. 2012. In vitro thermodynamic dissection of human copper transfer from chaperone to target protein. *PLoS One.* 7:e36102.
14. Mondol, T., J. Åden, and P. Wittung-Stafshede. 2016. Copper binding triggers compaction in N-terminal tail of human copper pump ATP7B. *Biochem. Biophys. Res. Commun.* 470:663–669.
15. Hamza, I., M. Schaefer, …, J. D. Gitlin. 1999. Interaction of the copper chaperone HAH1 with the Wilson disease protein is essential for copper homeostasis. *Proc. Natl. Acad. Sci. USA.* 96:13363–13368.
16. Arioz, C., Y. Li, and P. Wittung-Stafshede. 2017. The six metal binding domains in human copper transporter, ATP7B: molecular biophysics and disease-causing mutations. *Biometals.* 30:823–840.
17. Forbes, J. R., G. Hsi, and D. W. Cox. 1999. Role of the copper-binding domain in the copper transport function of ATP7B, the P-type ATPase defective in Wilson disease. *J. Biol. Chem.* 274:12408–12413.
18. Morin, I., S. Gudin, …, M. Cuillel. 2009. Dissecting the role of the N-terminal metal-binding domains in activating the yeast copper ATPase in vivo. *FEBS J.* 276:4483–4495.
19. Barry, A. N., A. Otoikhian, …, S. Lutsenko. 2011. The lumenal loop Met672-Pro707 of copper-transporting ATPase ATP7A binds metals and facilitates copper release from the intramembrane sites. *J. Biol. Chem.* 286:26585–26594.
20. Wittung-Stafshede, P. 2004. Role of cofactors in folding of the blue-copper protein azurin. *Inorg. Chem.* 43:7926–7933.
21. Palm-Espling, M. E., M. S. Niemiec, and P. Wittung-Stafshede. 2012. Role of metal in folding and stability of copper proteins in vitro. *Biochim. Biophys. Acta.* 1823:1594–1603.
22. Jones, J. A., D. K. Wilkins, …, C. M. Dobson. 1997. Characterization of protein unfolding by NMR diffusion measurements. *J. Biomol. NMR.* 10:199–203.
23. Berger, S., and S. Braun. 2004. 200 and More NMR Experiments: A Practical Course. Wiley-VHC, Weinheim, Germany.
24. Ponnandai Shanmugavel, K., D. Petranovic, and P. Wittung-Stafshede. 2017. Probing functional roles of Wilson disease protein (ATP7B) copper-binding domains in yeast. *Metallomics.* 9:981–988.
25. Gietz, R. D., and R. A. Woods. 2006. Yeast transformation by the LiAc/SS Carrier DNA/PEG method. *Methods Mol. Biol.* 313:107–120.
26. The UniProt Consortium. 2017. UniProt: the universal protein knowledgebase. *Nucleic Acids Res.* 45:D158–D169.
27. Krogh, A., B. Larsson, …, E. L. Sonnhammer. 2001. Predicting transmembrane protein topology with a hidden Markov model: application to complete genomes. *J. Mol. Biol.* 305:567–580.
28. Gourdon, P., X. Y. Liu, …, P. Nissen. 2011. Crystal structure of a copper-transporting PIB-type ATPase. *Nature.* 475:59–64.
29. Kelley, L. A., S. Mezulis, …, M. J. Sternberg. 2015. The Phyre2 web portal for protein modeling, prediction and analysis. *Nat. Protoc.* 10:845–858.
30. Dolinsky, T. J., J. E. Nielsen, …, N. A. Baker. 2004. PDB2PQR: an automated pipeline for the setup of Poisson-Boltzmann electrostatics calculations. *Nucleic Acids Res.* 32:W665–W667.
31. Yeghiazaryan, G. A., A. H. Poghosyan, and A. A. Shahinyan. 2005. Structural and dynamical features of hydrocarbon chains of dipalmitoylphosphatidylcholine (DPPC) molecules in phospholipid bilayers: a molecular dynamics study. *New Electronic Journal of Natural Sciences.* 1:44–50.
32. Kandt, C., W. L. Ash, and D. P. Tieleman. 2007. Setting up and running molecular dynamics simulations of membrane proteins. *Methods.* 41:475–488.
33. Hess, B., C. Kutzner, …, E. Lindahl. 2008. GROMACS 4: algorithms for highly efficient, load-balanced, and scalable molecular simulation. *J. Chem. Theory Comput.* 4:435–447.
34. Nagle, J. F. 1993. Area/lipid of bilayers from NMR. *Biophys. J.* 64:1476–1481.
35. Robertson, M. J., J. Tirado-Rives, and W. L. Jorgensen. 2015. Improved peptide and protein torsional energetics with the OPLSAA force field. *J. Chem. Theory Comput.* 11:3499–3509.
36. Berger, O., O. Edholm, and F. Jähnig. 1997. Molecular dynamics simulations of a fluid bilayer of dipalmitoylphosphatidylcholine at full hydration, constant pressure, and constant temperature. *Biophys. J.* 72:2002–2013.
37. Tieleman, D. P., J. L. Maccallum, …, L. Monticelli. 2006. Membrane protein simulations with a united-atom lipid and all-atom protein model: lipid-protein interactions, side chain transfer free energies and model proteins. *J. Phys. Condens. Matter.* 18:S1221–S1234.
38. Berendsen, H. J. C., J. P. M. Postma, …, J. Hermans. 1981. Interaction models for water in relation to protein hydration. *In* Intermolecular Forces: Proceedings of the Fourteenth Jerusalem Symposium on Quantum Chemistry and Biochemistry. B. Pullman, ed. Springer, pp. 331–342.
39. Bussi, G., D. Donadio, and M. Parrinello. 2007. Canonical sampling through velocity rescaling. *J. Chem. Phys.* 126:014101.
40. Nosé, S. 1984. A unified formulation of the constant temperature molecular-dynamics methods. *J. Chem. Phys.* 81:511–519.
41. Hoover, W. G. 1985. Canonical dynamics: equilibrium phase-space distributions. *Phys. Rev. A Gen. Phys.* 31:1695–1697.
42. Nosé, S., and M. L. Klein. 1983. Constant pressure molecular-dynamics for molecular-systems. *Mol. Phys.* 50:1055–1076.
43. Parrinello, M., and A. Rahman. 1981. Polymorphic transitions in single-crystals - a new molecular-dynamics method. *J. Appl. Phys.* 52:7182–7190.
44. Hess, B., H. Bekker, …, J. G. E. M. Fraaije. 1997. LINCS: a linear constraint solver for molecular simulations. *J. Comput. Chem.* 18:1463–1472.
45. Essmann, U., L. Perera, …, L. G. Pedersen. 1995. A smooth particle Mesh Ewald method. *J. Chem. Phys.* 103:8577–8593.
46. Wilkins, D. K., S. B. Grimshaw, …, L. J. Smith. 1999. Hydrodynamic radii of native and denatured proteins measured by pulse field gradient NMR techniques. *Biochemistry.* 38:16424–16431.

47. Kahra, D., M. Kovermann, and P. Wittung-Stafshede. 2016. The C-terminus of human copper importer Ctr1 acts as a binding site and transfers copper to Atox1. *Biophys. J.* 110:95–102.

48. Kovermann, M., P. Rogne, and M. Wolf-Watz. 2016. Protein dynamics and function from solution state NMR spectroscopy. *Q. Rev. Biophys.* 49:e6.

49. Kovermann, M., J. Ådén, …, M. Wolf-Watz. 2015. Structural basis for catalytically restrictive dynamics of a high-energy enzyme state. *Nat. Commun.* 6:7644.

50. Huster, D., A. Kuhne, …, S. Lutsenko. 2012. Diverse functional properties of Wilson disease ATP7B variants. *Gastroenterology.* 142:947–956.e5.

51. Maio, N., F. Polticelli, …, G. Musci. 2010. Role of external loops of human ceruloplasmin in copper loading by ATP7B and Ccc2p. *J. Biol. Chem.* 285:20507–20513.

52. Jayakanthan, S., L. T. Braiterman, …, S. Lutsenko. 2017. Human copper transporter ATP7B (Wilson disease protein) forms stable dimers *in vitro* and in cells. *J. Biol. Chem.* 292:18760–18774.

53. Schushan, M., A. Bhattacharjee, …, S. Lutsenko. 2012. A structural model of the copper ATPase ATP7B to facilitate analysis of Wilson disease-causing mutations and studies of the transport mechanism. *Metallomics.* 4:669–678.

54. Gourdon, P., O. Sitsel, …, P. Nissen. 2012. Structural models of the human copper P-type ATPases ATP7A and ATP7B. *Biol. Chem.* 393:205–216.

55. Sautron, E., C. Giustini, …, D. Seigneurin-Berny. 2016. Identification of two conserved residues involved in copper release from chloroplast PIB-1-ATPases. *J. Biol. Chem.* 291:20136–20148.